Superconductivity induced by electron doping in La_{1−x}M_{x}OBiS_{2} (M= Ti, Zr, Hf, Th)

D. Yazici, K. Huang, B. D. White, I. Jeon, V. W. Burnett, A. J. Friedman, I. K. Lum, M. Nallaiyan, S. Spagna, and M. B. Maple

Phys. Rev. B **87**, 174512 — Published 16 May 2013

DOI: 10.1103/PhysRevB.87.174512

Superconductivity induced by electron doping in the system $La_{1-x}M_xOBiS_2$ (M = Ti, Zr, Hf, Th)

D. Yazici[1,2], K. Huang[1,2,3], B. D. White[1,2], I. Jeon[1,2,3], V. W. Burnett[1,2], A. J. Friedman[1,2], I. K. Lum[1,2,3], M. Nallaiyan[4], S. Spagna[4], and M. B. Maple[1,2,3*]

[1]*Department of Physics, University of California, San Diego, La Jolla, California 92093, USA*

[2]*Center for Advanced Nanoscience, University of California, San Diego, La Jolla, California 92093, USA*

[3]*Materials Science and Engineering Program, University of California, San Diego, La Jolla, California 92093, USA and*

[4]*Quantum Design, 6325 Lusk Boulevard, San Diego, California 92121, USA*

(Dated: April 26, 2013)

We report a strategy to induce superconductivity in the BiS_2-based compound $LaOBiS_2$. Instead of substituting F for O, we increase the charge-carrier density (electron dope) via substitution of tetravalent Th^{+4}, Hf^{+4}, Zr^{+4}, and Ti^{+4} for trivalent La^{+3}. It is found that both the $LaOBiS_2$ and $ThOBiS_2$ parent compounds are bad metals and that superconductivity is induced by electron doping with T_c values of up to 2.85 K. The superconducting and normal states were characterized by electrical resistivity, magnetic susceptibility, and heat capacity measurements. We also demonstrate that reducing the charge-carrier density (hole doping) via substitution of divalent Sr^{+2} for La^{+3} does not induce superconductivity.

PACS numbers: 74.70.Dd, 74.25.F-, 74.25.Op

I. INTRODUCTION

Superconductivity with T_c = 8.6 K has recently been reported in the layered compound $Bi_4O_4S_3$.[1,2] Following this report, several other BiS_2-based superconductors, including $LnO_{1-x}F_xBiS_2$ (*Ln* = La, Ce, Pr, Nd, Yb) with T_c as high as 10 K, have been synthesized and studied.[3–12] These materials have a layered crystal structure composed of superconducting BiS_2 layers and blocking layers of $Bi_4O_4(SO_4)_{1-x}$ for $Bi_4O_4S_3$ and LnO for $LnO_{1-x}F_xBiS_2$ (*Ln* = La, Ce, Pr, Nd and Yb). This structural configuration is similar to the situation encountered in the high-T_c layered cuprate and Fe-pnictide superconductors, in which superconductivity primarily resides in CuO_2 planes and Fe-pnictide layers, respectively.[13–17] Even though BiS_2-based superconductors share a similar crystal structure with Fe-pnictide superconductors, they exhibit some important differences. The undoped parent compounds, *Ln*FeAsO, display a spin density wave (SDW) or a structural instability near 150 K.[15–17] Superconductivity emerges when the SDW is suppressed towards zero temperature either through charge carrier doping or application of pressure.[18] T_c is raised as high as 55 K by replacement of La by other rare-earth elements such as Sm.[15,16] In contrast, the phosphorus-based analogues *Ln*FePO do not show a SDW transition or structural instability but still exhibit superconductivity.[19,20] For LaFePO, values of T_c that range from 3 K to 7 K,[20,21] without charge carrier doping, have been reported. Both *Ln*FeAsO and *Ln*FePO remain metallic to low temperatures, while the undoped parent compounds $LnOBiS_2$ are bad metals. It has been suggested that superconductivity emerges in close proximity to an insulating normal state for the optimal superconducting sample.[11]

Several distinct examples of chemical substitution have been found to induce superconductivity in *Ln*FeAsO compounds including substituting F for O,[11,22–27] Co for Fe,[28] Sr for La,[29] Th for Gd,[30] and also the introduction of oxygen vacancies.[31,32] Substituting F for O induces superconductivity in BiS_2-based superconductors.[3,4,6–12,33–36] To determine whether superconductivity might emerge under other conditions, we chose to dope electrons via chemical substitution on the La site in $LaOBiS_2$. In this study, we demonstrate that substitution of tetravalent Th^{+4}, Hf^{+4}, Zr^{+4}, and Ti^{+4} for trivalent La^{+3} in $LaOBiS_2$ induces superconductivity. We also observed that substitution of divalent Sr^{+2} for La^{+3} (hole doping) does not induce superconductivity.

II. EXPERIMENTAL METHODS

Polycrystalline samples of $La_{1-x}Th_xOBiS_2$ ($0 \leq x \leq 1$), $La_{1-x}Hf_xOBiS_2$ ($0 \leq x \leq 0.4$), $La_{1-x}Zr_xOBiS_2$ ($0 \leq x \leq 0.3$), $La_{1-x}Ti_xOBiS_2$ ($0 \leq x \leq 0.3$), and $La_{1-x}Sr_xOBiS_2$ ($0 \leq x \leq 0.3$) were prepared by a two-step solid state reaction method using high-purity starting materials. Initially, the Bi_2S_3 precursor powders were prepared by reacting Bi and S grains together at 500 °C in an evacuated quartz tube for 10 hours. Starting materials of La, La_2O_3, S and Bi_2S_3 powders and either M = Th or Ti chunks, Hf granules, or Zr foil, were weighed in stoichiometric ratios based on nominal concentrations $La_{1-x}M_xBiS_2$ (M = Th, Hf, Zr, Ti). Next they were thoroughly mixed, pressed into pellets, sealed in evacuated quartz tubes, and annealed at 865 °C for 72 hours. Additional regrinding and sintering at 700 °C for 3 days was performed to promote phase homogeneity. The crystal structure was verified by means of x-ray powder diffraction (XRD) using a Bruker D8 Discover x-ray diffractometer with Cu-K_α radiation. The resulting XRD patterns were fitted via Rietveld refinement[37] using the GSAS+EXPGUI software package.[38,39] The chemical composition was investigated by means of energy dispersive x-rays (EDX) using a FEI Quanta 600 scanning electron microscope equipped with an INCA EDX detector from Oxford instruments. Electrical resistivity measurements were performed using a home-built probe in a liquid ^{4}He Dewar for temperatures 1 K $\leq T \leq$ 300 K by means of a standard four-wire technique using a Linear Research LR700 AC resistance bridge. Magnetization measurements were made for 2 K $\leq T \leq$ 300 K and in magnetic fields H = 5 Oe using a Quantum Design MPMS. AC

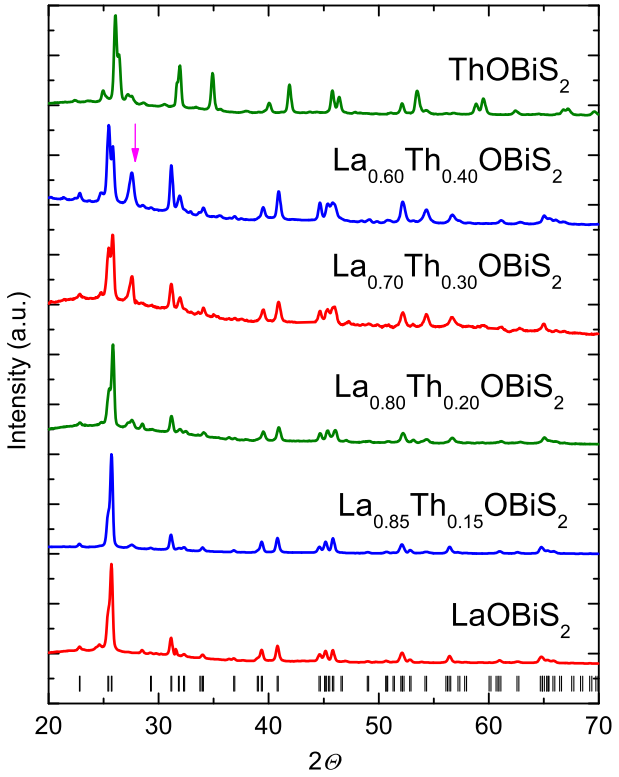

FIG. 1: (Color online) XRD patterns for selected concentrations of $La_{1-x}Th_xOBiS_2$ where values of x are explicitly labeled. The arrow indicates a Bi and/or Bi_2S_3 impurity.

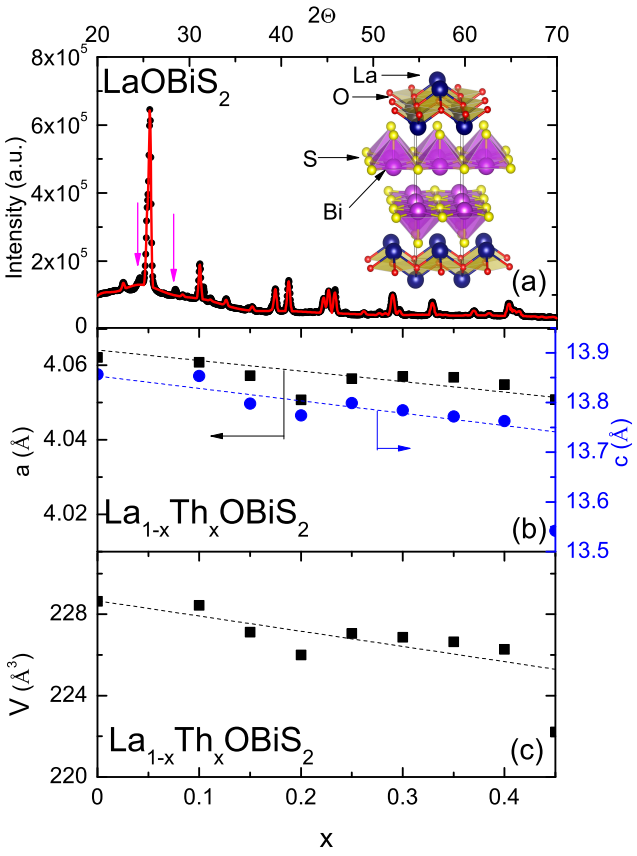

FIG. 2: (Color online) (a) X-ray diffraction (XRD) pattern for $LaOBiS_2$. Black circles represent data and the red solid line is the result of Rietveld refinement of the data. The arrows indicate a Bi and/or Bi_2S_3 impurity. (b) Lattice parameters a and c vs. nominal Th concentration x. (c) Unit cell volume V vs. nominal Th concentration x.

magnetic susceptibility was measured down to $\sim$ 1 K in a liquid ^{4}He Dewar. Specific heat measurements and electrical resistivity measurements under applied magnetic field for $La_{0.85}Th_{0.15}OBiS_2$ and $La_{0.8}Hf_{0.2}OBiS_2$ samples were performed for 0.36 K $\leq T \leq$ 30 K in a Quantum Design PPMS DynaCool with a ^{3}He insert using a thermal relaxation technique.

III. RESULTS

A. Crystal structure and sample quality

TABLE I: Crystallographic data for the compound $ThOBiS_2$ which was obtained from Rietveld refinement of a powder X-ray diffraction pattern collected at room temperature.

Chemical Formula		$ThOBiS_2$		
Space Group		P4 / nmm (No. 129)		
a (Å)		3.9623 (8)		
c (Å)		13.5062 (5)		
V (Å^3)		212.041 (6)		
Z		2		
Atom	site	x	y	z
Th	2c	0.25	0.25	0.1017(5)
Bi	2c	0.25	0.25	0.6013(2)
S1	2c	0.25	0.25	0.3080(17)
S2	2c	0.25	0.25	0.8382(12)
O	2a	0.75	0.25	0

Fig. 1 shows the powder XRD patterns of $LaOBiS_2$ and $ThOBiS_2$ samples. Overall, the main diffraction peaks of these two samples can be well indexed to a tetragonal structure with space group $P4/nmm$. The crystal structure has previously been designated as having the ZrCuSiAs type structure,[3–5,8] however, the $CeOBiS_2$ type structure may be a more appropriate structure assignment.[11] While the crystal

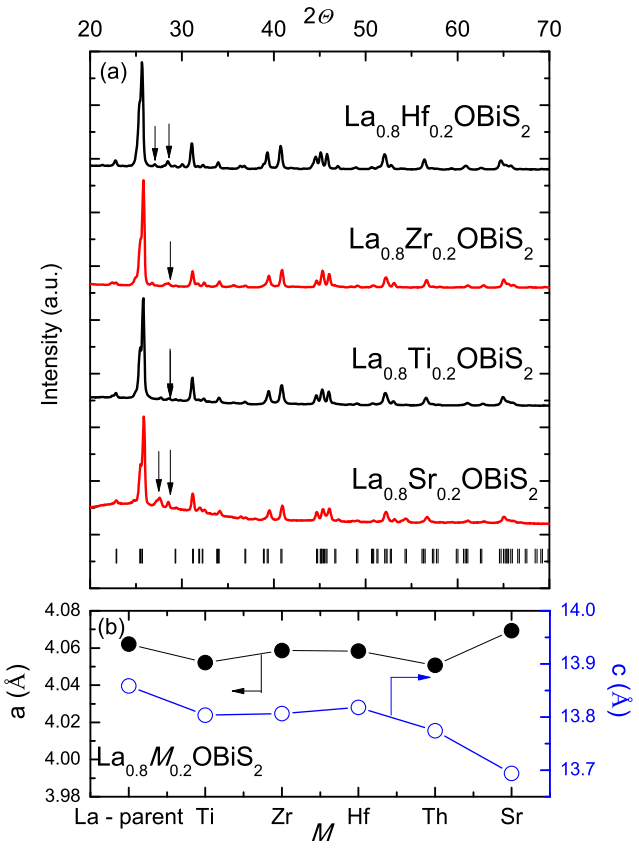

FIG. 3: (Color online) (a) XRD patterns and (b) lattice parameters a and c for $La_{1-x}M_xOBiS_2$ with M = Hf, Zr, Ti, Sr and $x = 0, 0.2$. The arrows indicate Bi and/or Bi_2S_3 impurities.

structure of $LaOBiS_2$ and $ThOBiS_2$ has a different Wyckoff sequence than that of ZrCuSiAs, it has the same Wyckoff sequence and positions, and similar unit cell parameter ratios (c/a) as the crystal structure for $CeOBiS_2$.[40] The crystallographic data for $ThOBiS_2$ obtained from Reitveld refinement of the powder XRD pattern given in Fig. 1 are tabulated in Table I. The inset of Fig. 2(a), displays the crystal structure of $LaOBiS_2$. The structure is composed of stacked La_2O_2 layers and two BiS_2 layers in each unit cell. To dope electrons into the BiS_2 conduction layers, we substituted tetravalent Th^{+4}, Hf^{+4}, Zr^{+4}, and Ti^{+4} for La^{+3} and to dope holes into the BiS_2 conduction layers, we substituted divalent Sr^{+2} for trivalent La^{+3}. We find that samples for the entire range of Th substitutions below the solubility limit, Hf substitutions in the range $0.1 \leq x \leq 0.4$, and Zr, Ti, and Sr substitutions in the range $0.1 \leq x \leq 0.3$, can be described by the same space group. As shown in Fig. 2(b), the lattice parameters a and c for $La_{1-x}Th_xOBiS_2$ ($0 \leq x \leq 1$) decrease with increasing Th concentration, although the relative decrease of a is much smaller than that of c. With Th doping, the positions of Bragg reflections shift systematically. For example, the (004) reflections shift to higher angles, consistent with a decrease of c. This result indicates that Th is really incorporated into the lattice; although, some amounts of elemental Bi and/or Bi_2S_3 separate from the lattice, indicated by arrows in Fig. 1 and Fig. 2(a). We could not always distinguish between whether the impurity phase was Bi or Bi_2S_3, since their Bragg reflections occur at very similar positions. If the impurity is assumed to be Bi, the amount is between 3% to 15% by mass and if the impurity is assumed to be Bi_2S_3, the amount is between 5% to 18% by mass. In either case, the ratio increases with increasing Th concentration. If the impurity is Bi, there should be other La-S-O based impurities, but we could not detect any elemental S or La impurities or binary compounds made from La-S-O. The impurity is therefore likely Bi_2S_3, which should be balanced with a La_2O_3 impurity. Unfortunately, the Bragg reflections of La_2O_3 overlap with the main phase peak positions, which makes it difficult to estimate the impurity ratio of La_2O_3 using Rietveld refinement. For $0.5 \leq x \leq 0.9$, the lattice parameters (not shown) are close to the lattice parameters of $ThOBiS_2$ and do not change appreciably with x. The impurity amount increases with x and other impurity peaks begin to appear in this region, indicating the probable existence of a solubility limit of La/Th near $x = 0.45$.

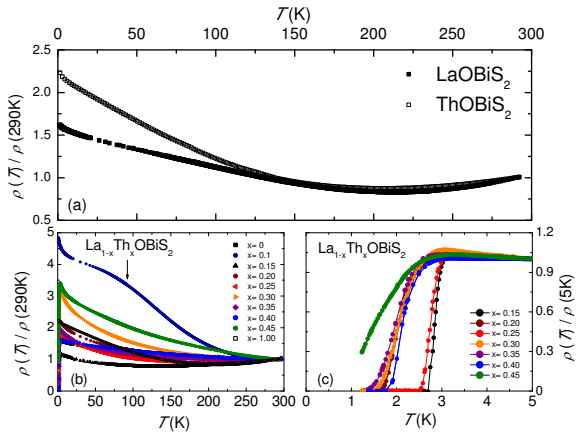

FIG. 4: (Color online) (a) Electrical resistivity ρ, normalized by its value at 290 K, vs. temperature T for $LaOBiS_2$ and $ThOBiS_2$. (b) ρ, normalized by its value at 290 K, vs. T for $La_{1-x}Th_xOBiS_2$ ($0 \leq x \leq 1$). (c) ρ, normalized to its value in the normal state at 5 K, vs. T emphasizing the transition into the superconducting state.

More direct evidence of Th incorporation into the lattice comes from chemical composition measurements by energy-dispersive X-ray (EDX) microanalysis. The EDX spectrum was collected from a single grain. Quantitative analysis for selected samples gives La:Th ratios of 0.08, 0.12, 0.18, and 0.24 for the samples with nominal ratios 0.1, 0.15, 0.20 and 0.25, respectively. This result demonstrates that most of the Th was successfully doped into the samples.

For the Hf, Zr, and Ti substitutions, the powder XRD patterns and lattice parameters a and c are given for $La_{1-x}M_xOBiS_2$ with M = Hf, Zr, Ti, Sr and $x = 0.2$ in Fig. 3(a) and Fig. 3(b), respectively. The lattice parameters a and c exhibit behavior similar to Th substitution, wherein the c lattice parameter decreases with increasing Hf, Zr, and Ti concentration and the a lattice parameter does not show

an appreciable concentration dependence. For Sr substitution, the a lattice parameter increases slightly, while c decreases with increasing Sr concentration. Even though the ionic size of Th is bigger than the others (Hf, Zr, and Ti), the c lattice parameters are very close to each other. The decrease of the c-axis may be attributed to a strengthening of the interlayer bonding as a consequence of doping.

B. Electrical resistivity

Electrical resistivity $\rho(T)$ data, normalized by the value of ρ at 290 K, are shown in Fig. 4 for the pure $LaOBiS_2$ and $ThOBiS_2$ samples. For both compounds, ρ initially decreases with decreasing temperature, exhibits a minimum at T = 220 K and T = 206 K, respectively, and then shows semiconductor-like behavior down to the lowest temperatures measured. For the $La_{1-x}Th_xOBiS_2$ system, the minimum in ρ is suppressed for $x = 0.1$, and $\rho(T)$ exhibits relatively strong temperature-dependence and an inflection point (indicated by an arrow) as shown in Fig. 4(b). For x = 0.15, this feature disappears and ρ drops to zero below T_c = 2.85 K. $\rho(T)$ becomes less temperature-dependent for $0.15 \leq x \leq 0.45$ and increases with decreasing temperature until the onset of superconductivity. First principles calculations have suggested that there may be a charge density wave instability or enhanced correlations in the $LaO_{1-x}F_xBiS_2$ system.[33] We are unable to unambiguously observe such an instability from the electrical resistivity measurements in this study. However, the inflection point could be related to such an effect.

Electrical resistivity measurements for $La_{1-x}Hf_xOBiS_2$, $La_{1-x}Zr_xOBiS_2$, and $La_{1-x}Ti_xOBiS_2$ samples are shown in Figs. 5, 6 and 7, respectively. Resistive superconducting

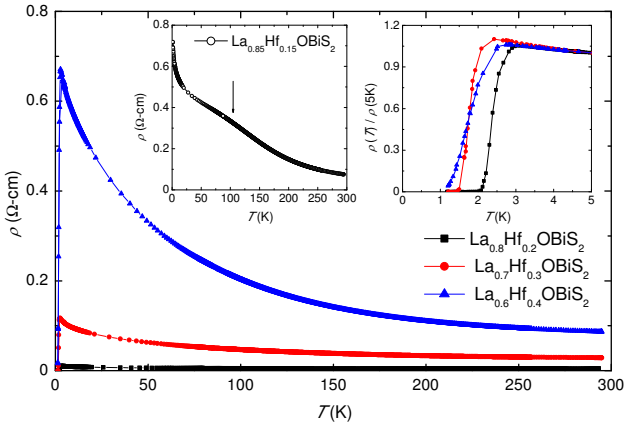

FIG. 5: (Color online) Electrical resistivity ρ vs. temperature T for $La_{1-x}Hf_xOBiS_2$. The left inset shows ρ vs. T for $La_{0.85}Hf_{0.15}OBiS_2$. The right inset displays the superconducting transition curves for samples with concentrations $0.2 \leq x \leq 0.4$.

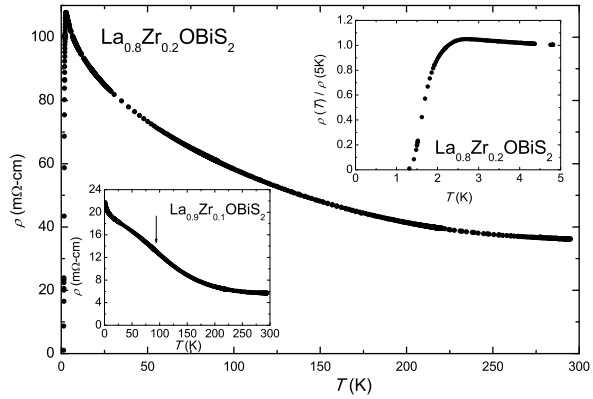

FIG. 6: Electrical resistivity ρ vs. temperature T, plotted for $La_{0.8}Zr_{0.2}OBiS_2$. The left inset shows ρ vs. T, for $La_{0.9}Zr_{0.1}OBiS_2$. The right inset displays the superconducting transition for $La_{0.8}Zr_{0.2}OBiS_2$.

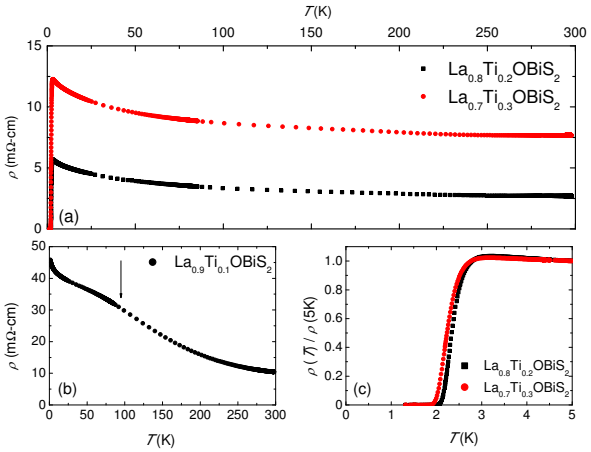

FIG. 7: (Color online) (a) Electrical resistivity ρ vs. temperature T, plotted for $La_{1-x}Ti_xOBiS_2$ ($x = 0.2 - 0.3$). (b) ρ vs. T for $La_{0.9}Ti_{0.1}OBiS_2$. (c) The superconducting transition curves for $x = 0.2 - 0.3$.

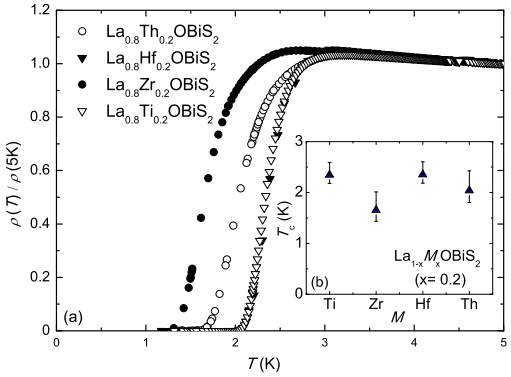

FIG. 8: (Color online) (a) The superconducting transition for 20% concentration of Th, Hf, Zr, and Ti. (b) Superconducting transition temperatures for $La_{1-x}M_xOBiS_2$ with M = Th, Hf, Zr, Ti and $x = 0.2$.

transition curves for these systems are indicated in the right inset of Figs. 5, 6, and 7(c). All of these doping studies show similar characteristics such as an inflection point anomaly in the normal state with low concentration and induced superconductivity for concentrations starting with x = 0.15 for $La_{1-x}Th_xOBiS_2$ and x = 0.2 for $La_{1-x}Hf_xOBiS_2$, $La_{1-x}Zr_xOBiS_2$, and $La_{1-x}Ti_xOBiS_2$. Furthermore, all of these systems show semiconductor-like behavior in the normal state. The inflection point in ρ of samples with low concentration is emphasized in the left inset of Figs. 5, 6, and in Fig. 7(b) where the anomaly is indicated by an arrow. These anomalies all appear to be present at a common temperature of roughly 120 K in concentrations x just below those where superconductivity is induced. To compare the superconducting transition temperatures (T_c) we consider data for 20% substitution of La by Th, Hf, Zr, and Ti in Fig. 8(a). The superconducting transition temperatures, as shown in Fig. 8(b), are characterized by the temperatures where the electrical resistivity drops to 50% of the normal state resistivity, and the width of the transition is determined by the temperatures where the resistivity drops to 90% and 10% of the normal state resistivity. Electron doping clearly induces superconductivity in $LaOBiS_2$. The T_c's are quite similar to one another, but the transition width is sharper for $La_{0.8}Hf_{0.2}OBiS_2$ and $La_{0.8}Ti_{0.2}OBiS_2$ than for $La_{0.8}Zr_{0.2}OBiS_2$ and $La_{0.8}Th_{0.2}OBiS_2$. The lowest T_c is seen in $La_{0.8}Zr_{0.2}OBiS_2$. There does not appear to be a clear correlation between T_c and the lattice parameters. Meanwhile, Fig. 9 shows $\rho(T)$ measurements for $La_{1-x}Sr_xOBiS_2$ wherein no evidence of a superconducting transition is observed down to ~ 1 K in the range $0.1 \leq x \leq 0.3$. This result suggests that hole doping is not sufficient to induce superconductivity. It is, however, interesting to note that the magnitude of ρ at low temperatures increases with increasing Sr concentration, which is similar to the behavior observed with Th, Hf, Zr, and Ti doping.

The temperature dependence of ρ, normalized by its value at 5 K for $La_{0.85}Th_{0.15}OBiS_2$ and $La_{0.8}Hf_{0.2}OBiS_2$ samples, is shown in Fig. 10(a, b), respectively, under several applied magnetic fields (H = 0, 0.01, 0.05, 0.1, 0.2, 0.3, 0.4, 0.5, 1, and 9 T) down to 0.36 K. Both samples undergo relatively sharp superconducting transitions at T_c = 2.85 K and T_c = 2.40 K for $La_{0.8}Th_{0.2}OBiS_2$ and $La_{0.8}Hf_{0.2}OBiS_2$, respectively. With increasing magnetic field, the transition width broadens and the onset of superconductivity gradually shifts to lower temperatures. Similar broadening of the transition was observed in the high-T_c layered cuprate and Fe-pnictide superconductors and attributed to the vortex-liquid state.[34,41] Fig. 10(c, d) shows the upper critical field H_c vs. T for $La_{0.85}Th_{0.15}OBiS_2$ and $La_{0.8}Hf_{0.2}OBiS_2$ samples, corresponding to the temperatures where the resistivity drops to 90% of the normal state resistivity $\rho_n(T,H)$ ($T_{c,onset}$), 50% of $\rho_n(T,H)$ (T_c), and 10% of $\rho_n(T,H)$ ($T_{c,zero}$) in applied magnetic fields. Using the conventional one-band Werthamer-Helfand-Hohenberg (WHH) theory,[42] the orbital critical fields $H_{c2}(0)$ for $La_{0.85}Th_{0.15}OBiS_2$ and $La_{0.8}Hf_{0.2}OBiS_2$ compounds were inferred from their initial slopes of H_c with respect to T, yielding values of 1.09 T and 1.12 T, respectively. These values of $H_{c2}(0)$, are very close to the values seen in $Sr_{1-x}La_xFBiS_2$ (1.04 T)[43] and $LaO_{0.5}F_{0.5}BiS_2$ (1.9 T),[8] suggesting that the superconducting state in BiS_2-based superconductors probably shares a common character.

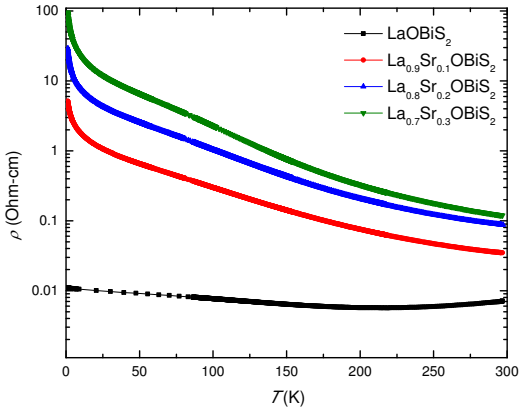

FIG. 9: (Color online) Electrical resistivity ρ vs. temperature T, for $La_{1-x}Sr_xOBiS_2$ $(0 \leq x \leq 0.3)$, plotted on a semi-log scale.

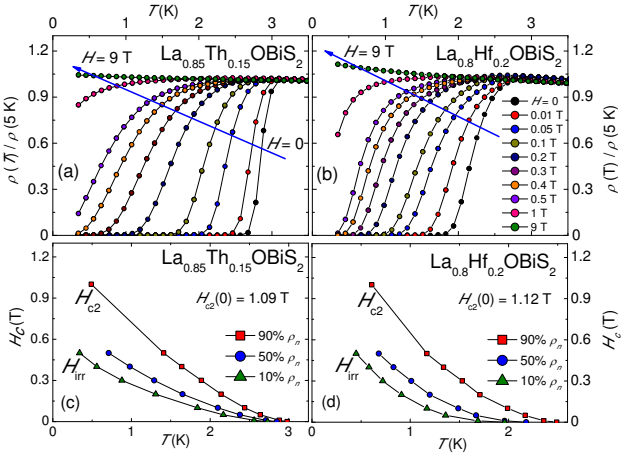

FIG. 10: (Color online) (a, b) Resistive superconducting transition curves for $La_{0.85}Th_{0.15}OBiS_2$ and $La_{0.8}Hf_{0.2}OBiS_2$ samples, respectively, measured under several different applied magnetic fields (H = 0, 0.01, 0.05, 0.1, 0.2, 0.3, 0.4, 0.5, 1, 9 T). (c, d) The temperature dependence of the upper critical field H_{c2}, and H_{irr}, determined from the 90% and 10% normal state ρ for $La_{0.85}Th_{0.15}OBiS_2$ and $La_{0.8}Hf_{0.2}OBiS_2$ samples, respectively. The temperature corresponding to the 50% normal state ρ is also shown.

C. Magnetization

To determine whether superconductivity is a bulk phenomenon in $La_{1-x}M_xOBiS_2$, zero field cooled (ZFC) and field cooled (FC) measurements of the magnetic susceptibility $\chi_{dc}(T)$ were made in a magnetic field of 5 Oe for

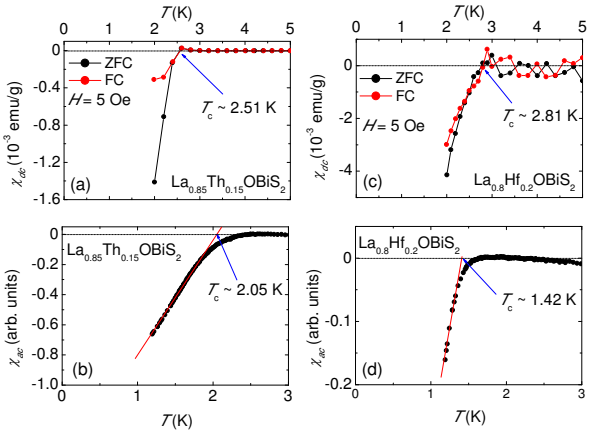

FIG. 11: (Color online) (a, c) DC magnetic susceptibility χ_{dc} vs. temperature T for $La_{0.85}Th_{0.15}OBiS_2$ and $La_{0.8}Hf_{0.2}OBiS_2$, respectively, measured in field cooled (FC) and zero field cooled (ZFC) conditions with a 5 Oe applied magnetic field. (b, d) Real part of the AC magnetic susceptibility χ_{ac} vs. T for $La_{0.85}Th_{0.15}OBiS_2$ and $La_{0.8}Hf_{0.2}OBiS_2$, respectively. The superconducting critical temperature T_c is indicated and labeled explicitly.

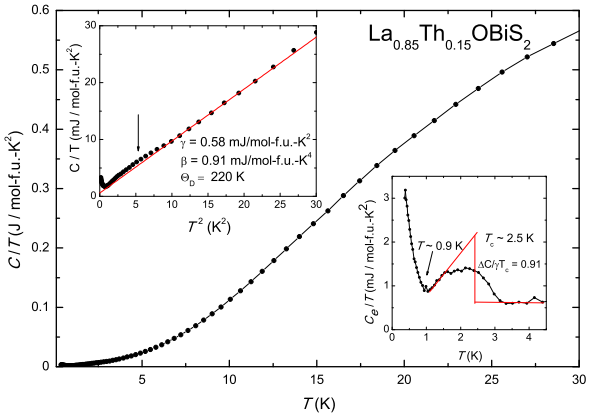

FIG. 12: Specific heat C divided by temperature T, C/T, vs. temperature T for $La_{0.85}Th_{0.15}OBiS_2$. C/T vs. T^2 is shown in the inset in the upper left hand part of the figure. The red line is a fit of the expression $C(T) = \gamma T + \beta T^3$ to the data which yields $\gamma = 0.58$ mJ/mol-f.u.-K^2 and Θ_D = 220 K. The inset in the lower right part of the figure shows a plot of C_e vs. T, where C_e/T is the electronic contribution to the specific heat, in the vicinity of the superconducting transition. An idealized entropy conserving construction yields T_c = 2.5 K and $\Delta C/\gamma T_c$ = 0.91.

the $La_{0.85}Th_{0.15}OBiS_2$ and $La_{0.8}Hf_{0.2}OBiS_2$ samples. These measurements are plotted in Fig. 11(a, c). ZFC measurements yield diamagnetic screening signals with T_c onset values that are lower than values obtained from $\rho(T)$ data, while FC measurements reveal evidence for strong vortex pinning. AC magnetic susceptibility measurements for $La_{0.85}Th_{0.15}OBiS_2$ and $La_{0.8}Hf_{0.2}OBiS_2$ samples are shown in Fig. 11(b, d), respectively. These data exhibit signatures of SC with slightly lower T_c's than those observed in ρ and χ_{dc} measurements. It is

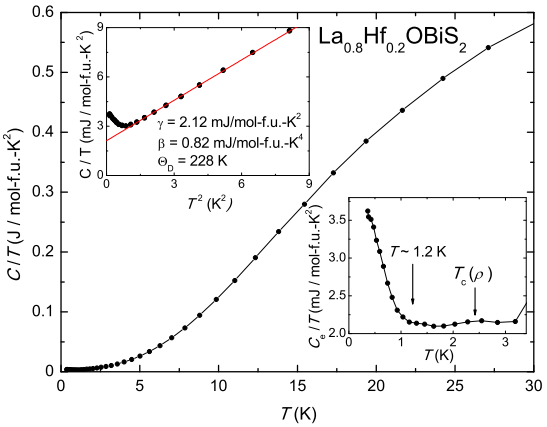

FIG. 13: Specific heat C divided by temperature T, C/T vs. temperature T $La_{0.8}Hf_{0.2}OBiS_2$. A plot of C/T vs. T^2 is shown in the inset in the upper left hand part of the figure. The red line is a fit of the expression $C(T) = \gamma T + \beta T^3$ to the data which yields $\gamma = 2.12$ mJ/mol-f.u.-K^2 and Θ_D = 228 K. A plot of C_e/T vs. T, in the vicinity of the superconducting transition, is displayed in the inset in the lower right hand side of the figure. The superconducting transition temperature T_c, obtained from the electrical resistivity measurements (T_c = 2.36 K), is indicated by an arrow.

clear that, even though the superconducting transition is incomplete at 1.3 K, the volume fractions are ∼67% and ∼16% for $La_{0.85}Th_{0.15}OBiS_2$ and $La_{0.8}Hf_{0.2}OBiS_2$ samples, respectively, according to the AC magnetic susceptibility measurements.

D. Specific heat

Specific heat data for $La_{0.85}Th_{0.15}OBiS_2$ and $La_{0.8}Hf_{0.2}OBiS_2$ samples are displayed in Fig. 12 and Fig. 13, respectively. The data for $La_{0.85}Th_{0.15}OBiS_2$ cover the temperature range 0.36 K to 30 K. A fit of the expression $C(T) = \gamma T + \beta T^3$ to the data in the normal state, where γ is the electronic specific heat coefficient and β is the coefficient of the lattice contribution, is plotted as a function of T^2 in the inset in the upper left hand side of Fig. 12. From the best fit, which is explicitly indicated by a line in the inset, we obtain values of $\gamma = 0.58$ mJ/mol-f.u.-K^2 and $\beta = 0.91$ mJ/mol-f.u.-K^4; the value of β corresponds to a Debye temperature of $\Theta_D = 220$ K. In the inset in the lower right hand side of Fig. 12, C_e/T vs. T is plotted. A clear feature is observed between 1 and 3 K. If this feature is related to the transition into the superconducting state, we can estimate T_c = 2.5 K from an idealized entropy conserving construction. This value of T_c is close to the temperature obtained from the electrical resistivity (T_c = 2.85 K). The presence of the feature may suggest that superconductivity is a bulk phenomenon in this compound. The ratio of the specific heat jump to γ T_c, $\Delta C/\gamma T_c$ = 0.91, was calculated using a jump in C_e/T of 0.53 mJ/mol-f.u.K^2, extracted from the entropy conserving construction as seen in the inset in the

lower right hand side of the figure. This value is less than the value of 1.43 predicted by the BCS theory, but is similar to that seen in $LaO_{0.5}F_{0.5}BiS_2$.[12]

The specific heat data for $La_{0.8}Hf_{0.2}OBiS_2$ are displayed between 0.36 K and 30 K in Fig. 13. The upper inset of Fig. 13 highlights the linear fit to the C/T data plotted vs. T^2, from which we extracted $\gamma = 2.12$ mJ/mol-f.u.-K^2 and $\beta = 0.82$ mJ/mol-f.u.-K^4, and calculated $\Theta_D = 228$ K. In the inset in the lower right hand side of the figure, the electronic contribution to the specific heat C_e/T vs. T is shown, which has been obtained by subtracting the lattice contribution βT^3 from $C(T)$. Absent from these data is any clear evidence for a jump at the T_c obtained from either the electrical resistivity or DC and AC magnetic susceptibility (T_c = 2.36 K, 2.81 K, and 1.42 K, respectively) measurements. However, there is a small feature around the T_c obtained from the electrical resistivity (T_c = 2.36 K) as indicated by an arrow in the lower right hand side of the figure. The absence of a well-defined superconducting jump at T_c is probably a consequence of the superconducting transition being spread out in temperature due to sample inhomogeneity.

There is an upturn in specific heat below roughly 1.2 K and 0.9 K for the $La_{0.8}Hf_{0.2}OBiS_2$ and $La_{0.85}Th_{0.15}OBiS_2$ samples, respectively. The same kind of upturn is also seen in $Sr_{0.5}La_{0.5}FBiS_2$ at a similar temperature. This upturn may be a contribution to specific heat from a Schottky anomaly or may be indicative of a second superconducting phase in this compound.[43] However, measurements must be made at temperatures below 0.36 K to unambiguously clarify the nature of this feature.

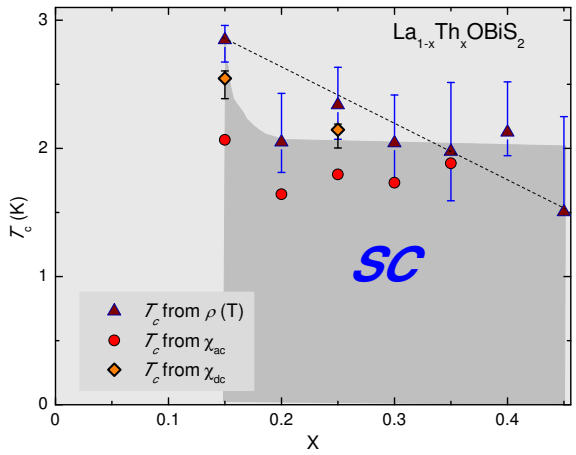

FIG. 14: (Color online) (a) Superconducting transition temperature T_c vs. Th concentration x phase diagram for the $La_{1-x}Th_xOBiS_2$ system. The phase diagram is constructed from electrical resistivity ρ (filled triangles), DC magnetic susceptibility χ_{dc} (filled diamonds), and AC magnetic susceptibility χ_{ac} (filled circles) measurements. The $T_c - x$ phase boundary (dark gray area) separates the superconducting phase (SC) from the normal phase. The value of T_c from $\rho(T)$ was defined by the temperature where ρ drops to 50% of its normal state value and vertical bars indicate the temperatures where the electrical resistivity drops to 90% and 10% of its normal state value. Values of T_c from χ_{ac} and χ_{dc} were defined by the onset of the superconducting transition. The dashed line indicates another possible upper bound for the SC region

IV. DISCUSSION

The results from $\rho(T)$, χ_{dc}, and χ_{ac} measurements are summarized in a phase diagram of T_c vs. Th concentration x shown in Fig. 14. $T_c(x)$ decreases with x from 2.85 K at x = 0.15 to 2.05 K at x = 0.20 and exhibits roughly concentration-independent behavior at higher concentration. The superconducting region may be defined by the dark gray region in Fig. 14, and apparently lacks a dome-like character typically seen for both the high-T_c layered cuprate and Fe-pnictide superconductors. Dome-like superconductor regions are also seen in $LaO_{1-x}F_xBiS_2$, and $NdO_{1-x}F_xBiS_2$.[6,9] At concentrations below the SC domes in these compounds, electrical resistivity measurements reveal bad metal or semiconducting-like behavior. These results are in agreement with first principles calculations[33] which suggest that the density of states at the Fermi level increases with increasing electron doping, such that the insulating parent compound becomes metallic. This effect is expected to be maximal at half filling (x = 0.5). The $LaO_{1-x}F_xBiS_2$ system[6] shows a maximum T_c for x = 0.5 while the $NdO_{1-x}F_xBiS_2$[9] system exhibits its highest T_c at x = 0.3. Other scenarios may be possible depending on how we define the SC region because of the broadness of the superconducting transitions. For example, a dashed line is also shown in Fig. 14 which mostly resides within the ranges characterized by the transition. In order to better define the phase boundary, studies on samples with sharper transitions would be beneficial.

A similar result can be seen in Fig. 15 where the highest $T_c(x)$ is observed at x = 0.2 for Hf, Zr and Ti doping. $T_c(x)$ decreases initially with increasing x and then becomes concentration-independent. The character of $T_c(x)$ observed for $La_{1-x}M_xOBiS_2$ and displayed in the phase diagram suggests that the superconducting state is similar for these systems. Considering other examples of inducing superconductivity by electron doping such as in $LaO_{1-x}F_xBiS_2$[4,6,8–10,12] and $Sr_{1-x}La_xFBiS_2$,[43] our results suggest that electron doping is a viable approach to induce superconductivity in BiS_2 based compounds.

V. CONCLUDING REMARKS

In summary, we have synthesized polycrystalline samples of $La_{1-x}M_xOBiS_2$ (M = Th, Hf, Zr, Ti, and Sr) with the $CeOBiS_2$ crystal structure. Electrical resistivity, DC and AC magnetic susceptibility, and specific heat measurements were performed on selected samples. Electron doping via substitution of tetravalent Th^{+4}, Hf^{+4}, Zr^{+4}, Ti^{+4} for trivalent La^{+3} induces superconductivity while hole doping via substitution of divalent Sr^{+2} for La^{+3} does not. These results strongly suggest that electron doping by almost any means may be sufficient to induce superconductivity in BiS_2-based compounds.

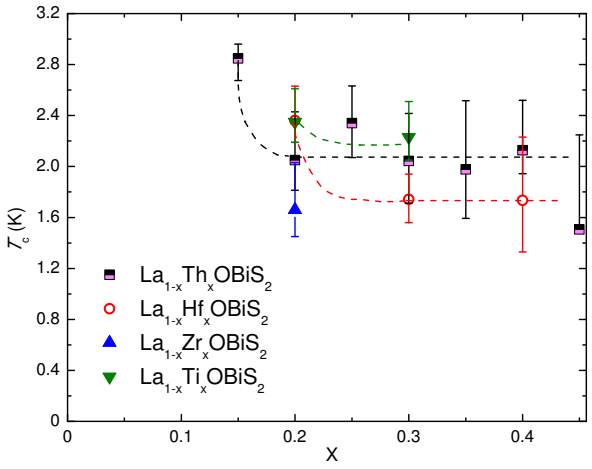

FIG. 15: (Color online) Superconducting transition temperature T_c vs. concentration x phase diagram for the $La_{1-x}M_xOBiS_2$ system (M = Th, Hf, Zr, Ti), constructed from electrical resistivity ($\rho(T)$) measurements. The value of T_c was defined by the temperatures where ρ drops to 50% of its normal state value and vertical bars are defined by the temperatures where ρ drops to 90% and of 10% of its normal state value.

Acknowledgments

The authors gratefully acknowledge the support of the US Air Force Office of Scientific Research - Multidisciplinary University Research Initiative under Grant No. FA9550-09-1-0603 and the US Department of Energy under Grant No. DE-FG02-04-ER46105.

* Corresponding Author: mbmaple@ucsd.edu

[1] Y. Mizuguchi, H. Fujihisa, Y. Gotoh, K. Suzuki, H. Usui, K. Kuroki, S. Demura, Y. Takano, H. Izawa, and O. Miura, Phys. Rev. B **86**, 220510(R) (2012).

[2] S. K. Singh, A. Kumar, B. Gahtori, S. Kirtan, G. Sharma, S. Patnaik, and V. P. S. Awana, J. Am. Chem. Soc. **134**, 16504 (2012).

[3] B. Li, Z. W. Xing, and G. Q. Huang, arXiv p. 1210.1743 (2012).

[4] R. Jha, A. Kumar, S. K. Singh, and V. P. S. Awana, J. Sup. and Novel Mag. **26**, 499 (2013).

[5] R. Jha, A. Kumar, S. K. Singh, and V. P. S. Awana, J. Appl. Phys. **113**, 056102 (2013).

[6] K. Deguchi, Y. Mizuguchi, S. Demura, H. Hara, T. Watanabe, S. J. Denholme, M. Fujioka, H. Okazaki, T. Ozaki, H. Takeya, et al., EPL **101**, 17004 (2013).

[7] H. Kotegawa, Y. Tomita, H. Tou, H. Izawa, Y. Mizuguchi, O. Miura, S. Demura, K. Deguchi, and Y. Takano, J. Phys. Soc. Jpn. **81**, 103702 (2012).

[8] V. P. S. Awana, A. Kumar, R. Jha, S. Kumar, A. Pal, Shruti, J. Saha, and S. Patnaik, Solid State Communication **157**, 23 (2013).

[9] S. Demura, Y. Mizuguchi, K. Deguchi, H. Okazaki, H. Hara, T. Watanabe, S. J. Denholme, M. Fujioka, T. Ozaki, H. Fujihisa, et al., J. Phys. Soc. Jpn. **82**, 033708 (2013).

[10] Y. Mizuguchi, S. Demura, K. Deguchi, Y. Takano, H. Fujihisa, Y. Gotoh, H. Izawa, and O. Miura, J. Phys. Soc. Jap. **81**, 114725 (2012).

[11] J. Xing, S. Li, X. Ding, H. Yang, and H.-H. Wen, Phys. Rev. B **86**, 2145181 (2012).

[12] D. Yazici, K. Huang, B. D. White, A. H. Chang, A. J. Friedman, and M. B. Maple, Philos. Mag. **93**, 673 (2012).

[13] J. Zhano, Q. Huang, C. D. L. Cruz, C. Li, J. W. Lynn, Y. Chen, M. A. Green, G. F. Chen, G. Li, Z. Li, et al., Nature Materials **7**, 953 (2008).

[14] L. Alff, Y. Krockenberger, B. Welter, R. Gross, D. Manske, and M. Naito, Nature (London) **422**, 698 (2003).

[15] J. Paglione and R. L. Greene, Nature Physics **6**, 645 (2010).

[16] D. C. Johnston, Advances in Physics **59** (2010).

[17] I. I. Mazin, Nature **464** (2010).

[18] H. Okada, K. Igawa, H. Takahashi, Y. Kamihara, M. Hirano, H. Hosono, K. Matsubayashi, and Y. Uwatoko, Journal of the Physical Society of Japan **77**, 113712 (2008).

[19] J. J. Hamlin, R. E. Baumbach, D. A. Zocco, T. A. Sayles, and M. B. Maple, Journal of Physics: Condensed Matter **20**, 365220 (2008).

[20] Y. Kamihara, H. Hiramatsu, M. Hirano, R. Kawamura, H. Yanagi, T. Kamiya, and H. Hosono, Journal of Physics: Condensed Matter **20**, 365220 (2008).

[21] M. Tegel, I. Schellenberg, R. Pöttgen, and D. Johrendt, Z. Naturforsch. B - Chem. Sci. **63**, 1057 (2008).

[22] Y. Kamihara, T. Watanabe, M. Hirano, and H. Hosono, Journal of the American Chemical Society **130**, 3296 (2008).

[23] G. F. Chen, Z. Li, D. Wu, G. Li, Z. Hu, J. Dong, P. Zheng, J. L. Luo, and N. L. Wang, Physical Review Letters **100**, 247002 (2008).

[24] Z. A. Ren, W. Lu, J. Yang, W. Yi, X. L. Shen, Z. C. Li, G. C. Che, X. L. Dong, L. L. Sun, F. Zhou, et al., Chinese Physics Letters **25**, 2215 (2008).

[25] Z. A. Ren, J. Yang, W. Lu, W. Yi, G. C. Che, X. L. Dong, L. L. Sun, and Z.-X. Zhao, Materials Research Innovations **12**, 105 (2008).

[26] Z.-A. Ren, J. Yang, W. Lu, W. Yi, X. L. Shen, Z. C. Li, G. C. Che, X. L. Dong, L. L. Sun, F. Zhou, et al., Europhysics Letters **82**, 57002 (2008).

[27] X. H. Chen, T. Wu, R. H. Liu, H. Chen, and D. F. Fang, Nature **453**, 761 (2008).

[28] A. S. Sefat, A. Huq, M. A. McGuire, R. Jin, B. C. Sales, D. Mandrus, L. M. D. Cranswick, P. W. Stephens, and K. H. Stone, Physical Review B **78**, 104505 (2008).

[29] H.-H. Wen, G. Mu, L. Fang, H. Yang, and Y. Zhu, Europhysics Letters **82**, 17009 (2008).

[30] C. Wang, L. Li, S. Chi, Z. Zhu, Z. Ren, Y. Li, Y. Wang, X. Lin, Y. Luo, S. Jiang, et al., Europhysics Letters **83**, 67006 (2008).

[31] Z.-A. Ren, G.-C. Che, X.-L. Dong, J. Yang, W. Lu, W. Yi, X.-L. Shen, Z.-C. Li, L.-L. Sun, F. Zhou, et al., Europhysics Letters **83**, 17002 (2008).

[32] J. Yang, Z.-C. Li, W. Lu, W. Yi, X.-L. Shen, Z.-A. Ren, G.-C. Che, X.-L. Dong, L.-L. Sun, F. Zhou, et al., Superconductor Science and Technology **21**, 082001 (2008).

[33] T. Yildirim, Phys. Rev. B **87**, 020506(R) (2013).

[34] J. Lee, M. B. Stone, A. Huq, T. Yildirim, G. Ehlers, Y. Mizuguchi, O. Miura, Y. Takano, K. Deguchi, S. Demura, et al., arXiv p. 1212.4811 (2012).

[35] I. R. Shein and A. L. Ivanovskii, arXiv p. 1211.3818 (2012).

[36] X. Wan, H.-C. Ding, S. Y. Savrasov, and C.-G. Duan, Phys. Rev. B **87**, 115124 (2013).

[37] H. M. Rietveld, J. Appl. Cryst. **2**, 65 (1969).

[38] A. C. Larson and R. B. Von Dreele, *General Structure Analysis System (GSAS)*, Los Alamos National Laboratory Report (1994).

[39] B. H. Toby, J. Appl. Cryst. **34**, 210 (2001).

[40] R. Ceolin and N. Rodier, Acta Crystallographica B **32**, 1476 (1976).

[41] H. Safar, P. L. Gammel, D. A. Huse, D. J. Bishop, J. P. Rice, and D. M. Ginsberg, Phys. Rev. Lett. **69**, 824 (1992).

[42] N. R. Werthamer, E. Helfand, and P. C. Hohenberg, Physical Review **147**, 1 (1966).

[43] X. Lin, X. Ni, B. Chen, X. Xu, X. Yang, J. Dai, Y. Li, X. Yang, Y. Luo, Q. Tao, et al., Phys. Rev. B **87**, 020504(R) (2013).